

Modeling of Mechanoelectrical Transduction of Hair Cells to Action Potentials in the Auditory Nerve

Anthony Au, Yuchen Wang, Sibai Xie

A Term Paper for BENG260

University of California, San Diego

San Diego, CA 92093

a5au@eng.ucsd.edu

wangyuchen0810@gmail.com

s8xie@eng.ucsd.edu

Abstract

An auditory nerve model based on Meddis model is test in this project. In this model, the input sound was decomposed into different constituent single frequencies, and was therefore responded by individual hair cells. Mechanical amplification during the transduction process was taken into account. The deflection was translated into the change in membrane potential, which was subsequently used as the input to the Meddis model. The spiking patterns were observed under pure tone and human voice stimulations. Phase-lock phenomenon, adaptation, and spiking rate pattern indicate that this model reflects some of the distinct properties of the hair cell.

1 Introduction

1.1 Hearing Mechanism of Human Ears

A human auditory system is one of the many examples of finely engineered functional systems that are fabricated by the nature. The sound wave is collected by an elegantly shaped auricle and introduces the vibration of the tympanum. Such vibration transmits through the three cartilaginous structures, malleus, incus and stapes, to the sound processing center of cochlea (Figure 1). The cochlea is the critical organism where mechanoelectrical transduction takes place [1].

1.2 Structure and functions of the human cochlea

The cochlea forms a spiral structure, and if we unfold it, we obtain a strip-like structure. The detailed structure of cochlea is very complicated, so in this project we only focus on the hair cell behavior in the cochlea (Figure 2). There are thousands of hair cells in the cochlea, between the tectorial membrane and the basilar membrane. They are specialized sensory epithelial cells. Two types of hair cells are present: inner hair cells (IHCs) and outer hair cells (OHCs). OHCs are believed to play a role in the active amplification process, and also the decomposition of complex sound [6]. In this project, we focus on the mechanoelectrical transduction that is realized by IHCs. The sound decomposition function of OHC is mimicked by a Fourier transform and threshold filtering process.

1.3 Inner Hair cells

The hair cells in different positions on the cochlea respond to different frequencies of sound. It is found that the hair cells in the deeper position of the cochlea are stiffer and respond to lower frequencies of sound. The heights of the stereocilia also increase from the base to the apex of the cochlea. This together with gradual change in the thickness of the basilar membrane gives rise to the sensitivity to a broad range of frequencies. The sound wave triggers the movement the vibration of the basilar membrane, and subsequently causes the hair cells to move against the stationary tectorial membrane. The deflection of hair bundle or the bundle of the stereocilia and kinocilia leads to the opening of the potassium channel by a tip link connecting the top of every stereocilium. This unique mechanical gating mechanism ensures the sensitivity of the system to the rapid change in the frequency of the sound.

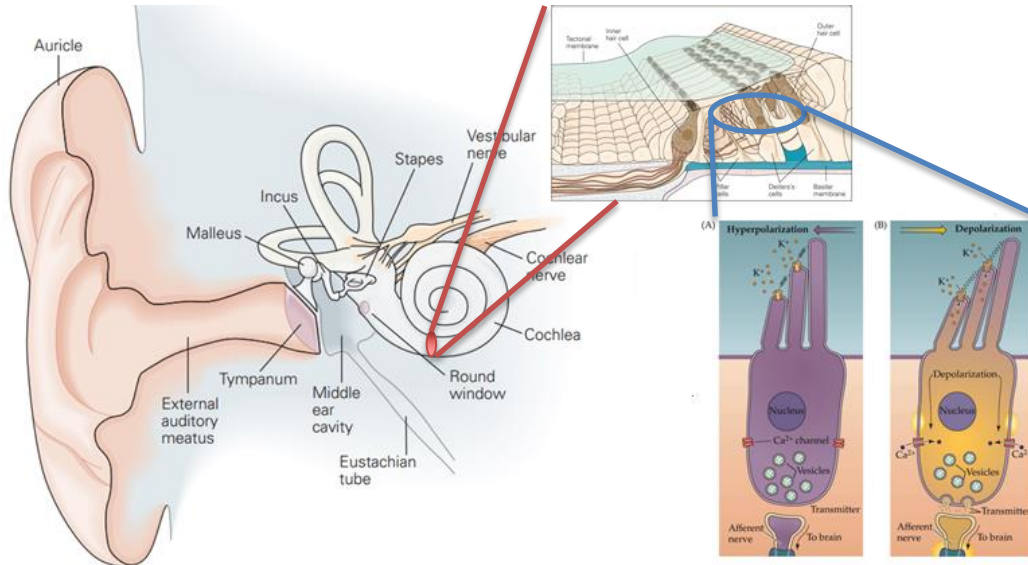


Figure 1: The structure of a human ear. The hair cells sit in the middle of tectorial and basilar membranes. The structure of the hair cell is shown on the right. When hair cell bundles are deflected, the tip links trigger the potassium gates to open up.

2 Model Description

2.1 Frequency analysis

In order to know how many hair cells join the encoding of the sound. The original sound is firstly transformed through Fourier transform into the frequency domain. Then a threshold was set based on the Gaussian white noise assumption to filter out the noise and pick out the major frequency components which indicates the number of active hair cells. An assumption was made here that one hair cell only responded to one specific frequency.

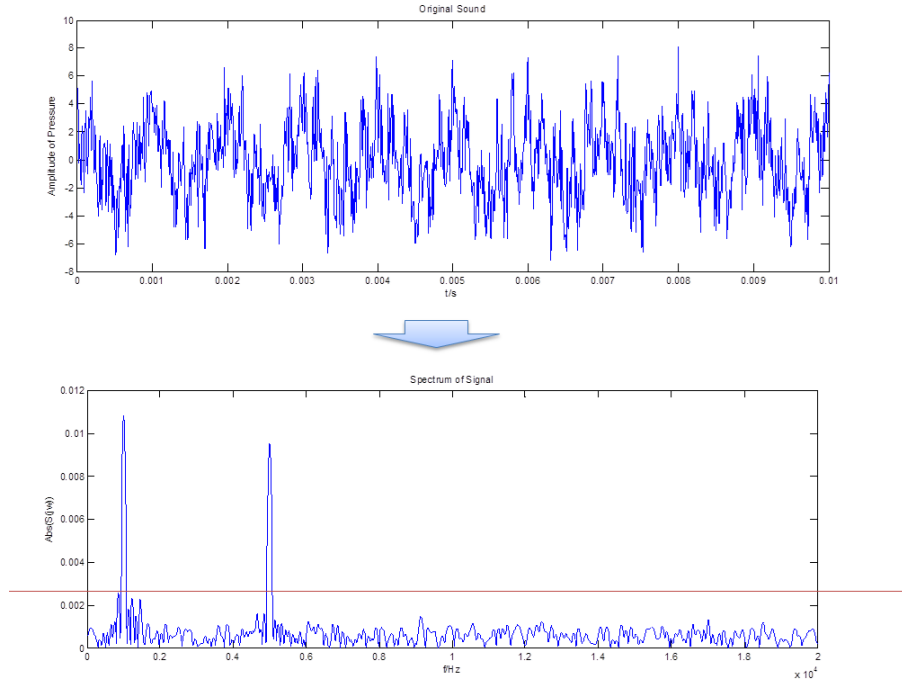


Figure 2: Fourier transform of the original signal and threshold setting.

(The red line in the lower graph is a demonstration of a threshold and it equals to the mean of the amplitude of the signal plus the three times standard deviation).

2.2 Sound pressure conversion to membrane potential

The following equations were used for calculating the deflection and the resulting membrane potential changes. The mechanical vibration is sent to cochlea and the force of sound pressure is converted to deflection by equation 1. The denominator of the equation is a combination of the tip link stiffness ($N\gamma^2\kappa$) and a position-dependent hair bundle stiffness (K_{sp}). The deflection is then used to calculate the membrane voltage change by equation 2. This equation was subtracted from experimental results [1].

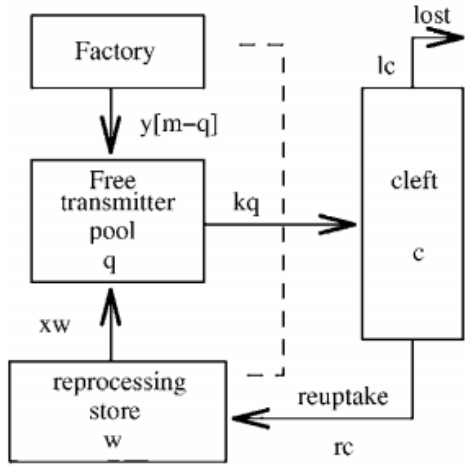
$$\Delta X = \left(\frac{1}{N\gamma^2\kappa + K_{sp}} \right) \Delta F_{HB} \quad (1)$$

$$V_m = \frac{20.2734}{5.7578 * e^{\left(\frac{\Delta X}{24.73}\right)} + 1} - 60 \quad (2)$$

2.3 Meddis model for hair cell synapse

In 1986, Meddis published his hair cell ribbon synapse model [2]. The model consists of four parts: factory, free transmitter pool, reprocessing store, cleft. The factory is the source of the transmitters and these transmitters will flow to the free transmitter pool with a speed proportional to the amount of the remaining transmitters. When the membrane potential of the presynaptic neuron changes, the neurotransmitters will leak from the free transmitter pool into the Cleft to incite the spiking of postsynaptic neuron and the speed is controlled by the presynaptic neuron's membrane potential and concentration of transmitters in the pool. During this process, some of transmitters will be lost because of the random motion and some will be reuptake by reprocessing store which then replenishes the free transmitter pool after being fixed. In the end, the remaining transmitters will exert influences on the postsynaptic neuron. For the purpose of simplifying the problem, we assume that one

transmitter causes a spike. Then the releasing rate is the spike rate at each moment.



The differential equations describing this model are shown below:

$$\frac{dq}{dt} = xw(t) + y(M - q(t)) - k(t)q(t)$$

$$\frac{dc}{dt} = k(t)q(t) - lc(t) - rc(t)$$

$$\frac{dw}{dt} = rc(t) - xw(t)$$

$$k(t) = g * dt[s(t) + A]/[s(t) + A + B]$$

when $[s(t) + A] > 0$

$$k(t) = 0 \text{ when } [s(t) + A] < 0$$

Figure 3: Schematic description of the Meddis model [3]

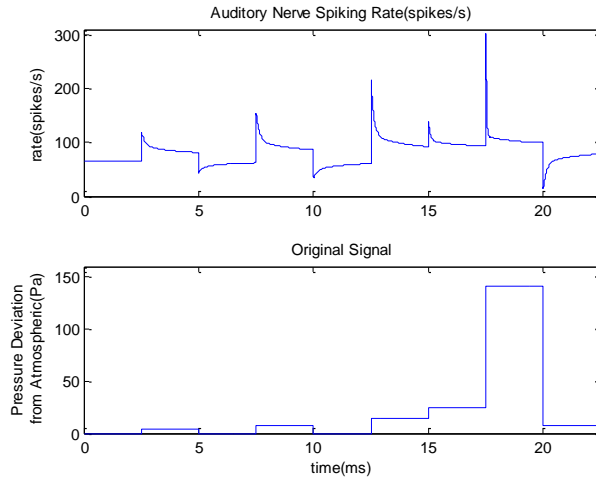


Figure 4: Meddis Model with a step function input signal

We demonstrated the adaptability of the Meddis model by using a step function as the input signal. When the first step in the signal occurs at 2.5ms, the model responds with a spike rate that eventually declines due to adaptation to the constant stimulus. When the stimulus is removed, the model responds with an offset adaptation (the signal dips below the initial zero stimulus point before rising back to the steady state point for the stimulus intensity). At 15ms, the stimulus is increased from a non-zero value and the model responds by showing a short increase in spiking rate before settling into the new steady state. A similar phenomenon is shown again when the stimulus increases at 17.5ms. Thus, this model shows the ability to adapt to louder or softer sounds.

3 Results and discussion

3.1 Pure tones analysis

Pure tone was firstly used to test the validity of our model and the phenomenon our model can reflect. In the test we used a 50dB, 1 kHz pure tone with a 30dB Gaussian white noise. The waveform and the frequency domain are shown in Figure 5. After processing by our model, the final spiking pattern is shown in Figure 6.

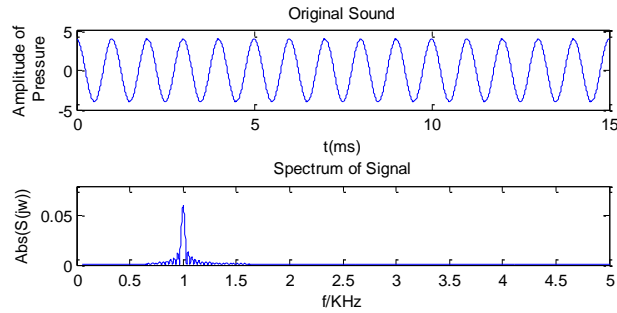


Figure 5: Pure tone waveform and its frequency components

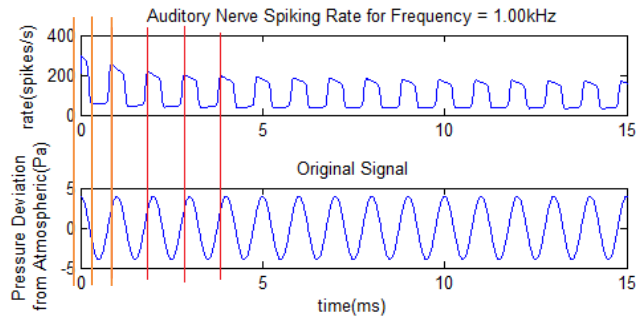


Figure 6: Spiking pattern of the hair responding to the pure tone.

Firstly the figure shows that the model successfully picks up the pure tone signal without being influenced by noise and it also displays two important phenomena – phase locking and adaptation.

As the red lines indicate, the auditory neuron’s spike rate reaches its maximum value at the same portion of each pure tone cycle. In another words, the response (spike pattern) is aligned with the stimulus periods. This is the phase locking which has been tested by the experiment in auditory neurons [4].

The figure also shows that in each stimulus cycle, the auditory neuron reaches the local maximum spiking rate first and then decreases its spiking rate, even though the strength of the stimulus is still increasing. The local maximum value of each cycle also decreases as the stimulus continues until it finally reaches a steady state. The former phenomenon is called short-term adaptation (shown earlier in figure 4) and the second one is long-term adaptation. They are both the basic phenomenon in the auditory experiments which further prove the validity of the model.

Comparing with the adaptation, why the model can reflect the phase-locking is easier to understand. As the transforms we used for the sound, pressure and deflection are linear transform, the phase-locking seems to be natural result.

The occurrence of adaptation is a little strange at first, but it can be explained by the Meddis model. For each period, the hair cell rapidly consumes transmitters when its membrane potential deviates from the resting value. When the reprocessing store can’t replenish the free pool in time, the short-term adaptation occurs and the spiking rate has to decrease. And for the lasting loss of transmitter by the cleft, the neuron’s maximum spike rate in each cycle decreases. Moreover, it can be better shown by the solution of the Meddis model’s differential equations.

In fact, the k in the equation should be a function of the hair cell’s membrane potential and the equations are nonlinear. But when the frequency of the sound is very high, k can be treated as a constant [3]. Then assuming the initial conditions for the variables are all zero and applying the Laplace transform to the equation, the results are:

$$Q(s) = \frac{(s + y + k)(s + x)(s + l + r)yM}{s((s + y + k)(s + k)(s + l + r) - xrk)}$$

Because the dominator of $Q(s)$ is a forth order polynomial. The inverse Laplace transform of it should be of the form:

$$q(t) = \text{Const} + C_1 e^{\frac{-t}{t_1}} + C_2 e^{\frac{-t}{t_2}} + C_3 e^{\frac{-t}{t_3}} \quad t \geq 0$$

In the solution, the relatively smaller t_i accounts for the short term adaptation while the larger t_i causes the long-term adaptation. Moreover, when time goes to infinity, $q(t)$ reaches the steady value.

3.2 Two-frequency tone analysis

In this section, two-frequency tones are used to test the robustness of the model. Here we use two 50dB tones with frequencies: 1 kHz and 5 kHz. The analysis result are shown in Figure 7

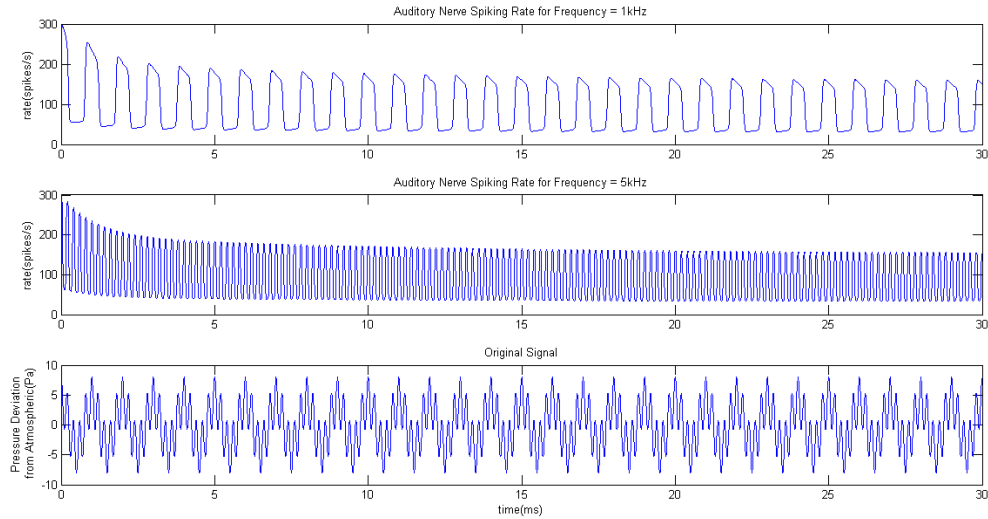


Figure 7: Two-frequency tone analysis result. (The first and second graph are spiking patterns of two auditory neurons. The third one is the original sound)

The figure shows that the model successfully picks out the two major frequency components and the spiking patterns basically reflect the phase-locking and adaptation.

Plotting the first local maximum value of two neurons with the frequency spectrum of the original sound together and normalize them results in figure 8.

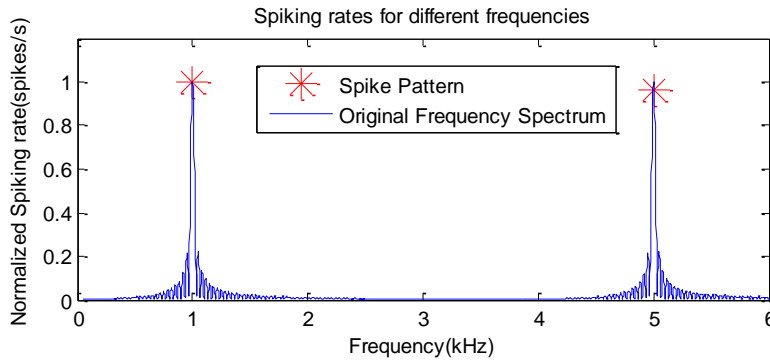


Figure 8: The normalized frequency spectrum. (The two red dots represent first local maximum spiking rates of two neurons)

As figure 8 shows, the normalized firing rate of neurons can reflect the frequency spectrum of the original sound in certain degree. Actually, this is an important characteristic of auditory neuron encoding and the details will be discussed in the next section

3.2 Complex Signal

We simulated the model with a complex signal in order to test its ability to respond to the type of sounds commonly detected by human inner hair cells. The complex signal was a short .wav file recording of a group member speaking the phrase “Good Morning”. Although simple, this phrase still contained many different frequencies along with background noise.

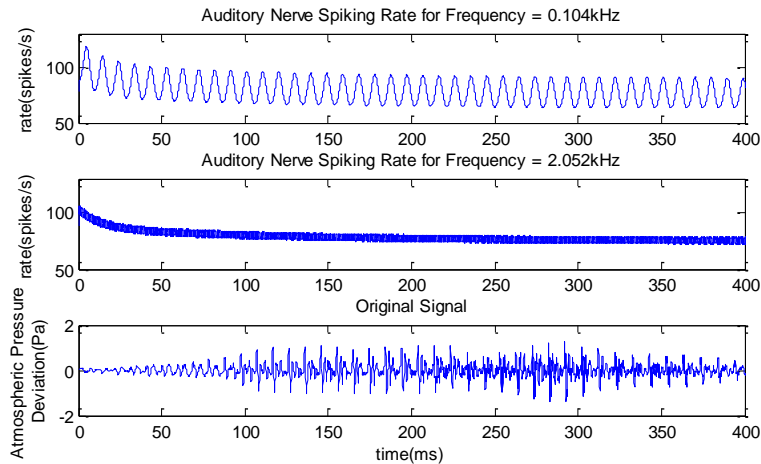


Figure 9: Spiking rates for the highest and lowest frequencies detected by our model

The spiking rate analysis of the complex signal showed similar results as both the single pure tone and the two pure tones signals. As the signal continues the spiking rates decrease, which demonstrates the adaptation showed earlier. The complex signal contained significantly more frequencies, but they all displayed similar adaptation results. We were unable to determine phase locking due to the difficulty associated with the mass frequencies and background noise of the original signal.

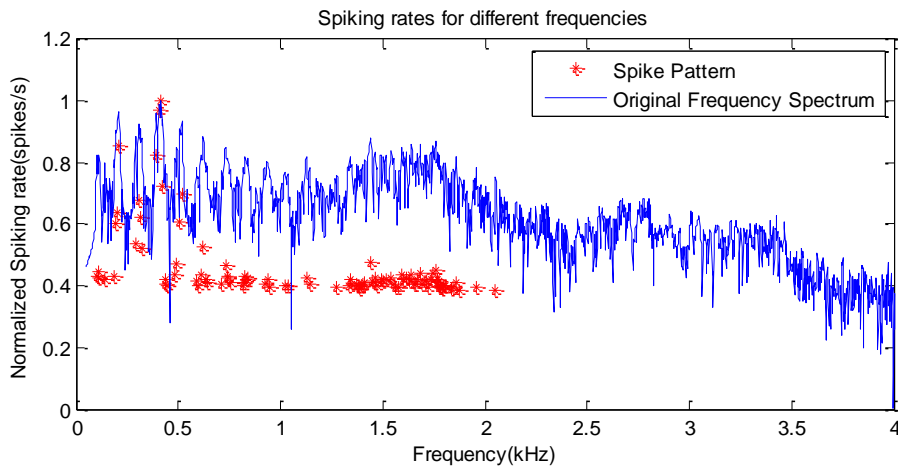


Figure 10: The Normalized Spiking Rates for the frequency spectrum isolated at the first local minimum of the spiking rates (shown in figure 9 above)

As shown in figure 8, the normalized firing rate of neurons can reflect the frequency spectrum. The complex frequency displays similar results. Each point signifies the spiking rate of an individual frequency isolated at the point where the first local maximum occurs. We chose to isolate the rates at the time the first local maximum occurred instead of at 0ms (start of the signal) because the beginning spiking rate was affected by the initial conditions and did not accurately display the dynamics of the hair cell. The first local maximum offered an easy point to determine

that each spiking rate vs frequency plot had in common. In figure 10, it can be seen that the pattern created by the spiking rates has a similar wave form to the first portion of the normalized frequency spectrum. There are no points after 2 kHz because those frequencies were filtered out as noise by the model. The amplitude of the spiking rates is lower than that of the actual frequency spectrum but this may be due to only one hair cell responding to each signal and a lack of amplification of the original signal. This reflection replicates a similar physiological phenomenon, where the spiking rates of different hair cells have a similar pattern to the frequency spectrum of the original signal [5].

4 Conclusions and future steps

4.1 Conclusions

The spiking patterns were observed under pure tone and human voice stimulations. Phase-lock phenomenon, adaptation, and spiking rate pattern indicate that this model reflects some of the distinct properties of the hair cell. The pure tone analysis shows that our model can successfully pick up the responding hair cell and transform the original sound to the final spiking pattern of the hair cell. More importantly, it can reflect two key physiological phenomena – phase locking and adaptation. The complex signal displayed similar adaptation characteristics to both of the pure tone analyses. By using the complex signal, we were also able to demonstrate the strength of the model in replicating the physiological phenomenon of the spiking rates following the frequency spectrum. Overall, this model approximates several distinct properties of hair cells in decoding sound signals and encoding action potentials to reflect these signals. This model may be used to further explore the auditory system and assist in the development of a fully functional ear.

4.2 Future steps

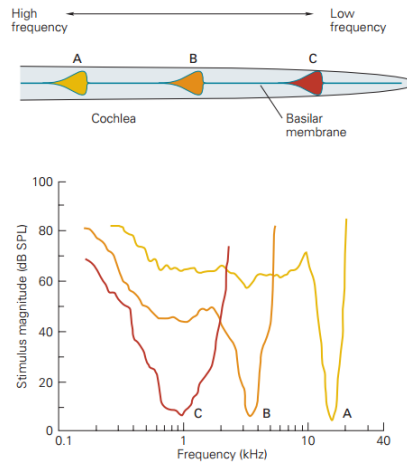


Figure 11: Range of frequency responses of 3 different hair cells for varying stimulus intensity

As shown in figure 11, each hair cell may respond to multiple frequencies. At the threshold intensity the hair cells may only respond to a single frequency, but as the intensity of the signal is increased (volume), the hair cells respond to a broader range. This phenomenon suggests that multiple hair cells are responsible detecting a certain frequency. As a result, the spike train for that specific frequency may be the spatial summation of several hair cells. In future works, we would like to include this phenomenon in our model. This should result in more spikes per second in the post stimulus time histogram, since more action potentials will be created by the multiple hair cells responding to each frequency. A spatial summation of the action potentials created from the different hair cells would allow for a more physiologically relevant model and offer better insights into how the signals ultimately encoded for interpretation by the auditory cortex.

References

- 1 James H. Schwartz, et al., *Principles of Neural Science*. 5th edn (McGraw-Hill, 2013).
- 2 R. Meddis, 'Simulation of Mechanical to Neural Transduction in the Auditory Receptor', *Journal of the Acoustical Society of America*, 79 (1986), 702-11.
- 3 R. Meddis, M. J. Hewitt, and T. M. Shackleton, 'Implementation Details of a Computation Model of the Inner Hair-Cell Auditory-Nerve Synapse', *Journal of the Acoustical Society of America*, 87 (1990), 1813-16.
- 4 J. E. Rose, J. F. Brugge, D. J. Anderson, and J. E. Hind, 'Phase-Locked Response to Low-Frequency Tones in Single Auditory Nerve Fibers of Squirrel Monkey', *Journal of Neurophysiology*, 30 (1967), 769-&.
- 5 M. B. Sachs, and E. D. Young, 'Encoding of Steady-State Vowels in the Auditory-Nerve - Representation in Terms of Discharge Rate', *Journal of the Acoustical Society of America*, 66 (1979), 470-79.
- 6 A. Stasiunas, et al., 'Compression, Adaptation and Efferent Control in a Revised Outer Hair Cell Functional Model', *Medical Engineering & Physics*, 27 (2005), 780-89.

Appendix: Values used for the variables in the model

Variable	Value	Variable	Value
A	5	Basic_Pressure	$2 \cdot 10^{(-5)}$ N/m ²
B	300	Oval window amplification	22.4
g	2000	$N\gamma^2\kappa$	6000 uN/m
y	5.05	Ksp	1000 uN/m
l	2500	H	50000
x	66.3		
r	6580		
m	1.0		